Optimization of Simulation Parameters for Wet Concrete Particles Based on Response Surface Methodology and PSO-BP-GA Method

Xiaohui Liu[1,2]✉ – Siyu Dong[1,2] – Kaidong Xue[1,2] – Penghui Wang[1,2] – Yongyi Ren[3]

[1] School of Construction Machinery, Chang'an University, China
[2] Key Laboratory of Road Construction Technology and Equipment of MOE, Chang'an University, China
[3] Xi'an Aerospace Precision Electromechanical Institute, China

✉ chd160039@chd.edu.cn

Abstract *To address the challenges of low calibration efficiency and limited accuracy in the discrete element modeling of wet concrete within high-dimensional parameter spaces, this study developed a parameter calibration scheme that integrates experimental design and intelligent algorithms. It achieved efficient and high-precision inverse function optimization for determing contact parameters, thereby providing a robust foundation for related engineering simulations. Specifically, the repose angle of wet concrete was determined to be 32.07° based on the heap experiment. Through the Plackett-Burman (PB) experiment and steepest ascent experiment, the three parameters with the greatest influence on the repose angle of wet concrete and their optimal value ranges were identified. These parameters are static friction (X_1), the coefficient of rolling friction (X_2), and surface energy (X_3). Subsequently, using the Box-Behnken (BB) test, the optimal 17 sets of combined data for these three significant factors were determined. To establish the objective function between the repose angle of wet concrete and its influencing parameters, and to obtain optimal parameter values, the particle swarm optimization (PSO) - back propagation (BP) - genetic algorithm (GA) method (PSO-BP-GA) is adopted. First, 80 % of the 17 sets obtained from the BB test were used as the training samples for the BP neural network (BPNN), while the remaining 20 % served as test samples. Then, the PSO is used to optimize the weights and thresholds within the BPNN. After deriving the objective function, GA was utilized to perform inverse function optimization, targeting repose angle of 32.07°. Finally, the static friction coefficient (X_1) between wet concrete particles was determined to be 0.158, the rolling friction coefficient (X_2) 0.187, and the surface energy (X_3) 1.580 J/m^2. With these parameters, five simulations were conducted, yielding an average repose angle of 32.31°. Compared with the actual repose angle, the relative error was 0.748 %.*

Keywords *wet concrete particles, particle simulation parameter optimization, response surface analysis, PSO-BP-GA*

Highlights

- *The parameters affecting the repose angle and their ranges were identified using the Plackett-Burman and steepest ascent experiments.*
- *The influence and ranking of these parameters on the repose angle were determined using the Box-Behnken test.*
- *The BPNN was then optimized using particle swarm optimization, and the objective function for the repose angle was obtained.*
- *The optimal parameter values in the objective function were determined using genetic algorithm.*

1 INTRODUCTION

The discrete element method (DEM), a powerful numerical simulation tool [1-3], has been widely utilized in the studies of particle materials. In this paper, the Hertz-Mindlin with Johnson-Kendall-Roberts (JKR) contact model [4-6], which is commonly employed in wet particle simulations, is adopted to model wet concrete particles. Nevertheless, the accuracy of the DEM approach is highly reliant on the precise calibration of the contact parameters between particles. To obtain the optimal simulation parameters for wet concrete particles, it is essential to identify which parameters should be optimized and to define the appropriate objective function.

When the optimization parameters and their feasible ranges are undetermined, traditional methods such as analysis of variance (ANOVA) [7] and stepwise regression [8] often suffer from low efficiency, and a high risk of misjudgment or omission when dealing with multi-dimensional parameters and complex models. To avoid these limitations, a combined experimental strategy incorporating the Plackett-Burman (PB) experiment and the steepest ascent experiment [9-12] can be adopted. This approach can rapidly identify the most influential parameters on the experiment and their corresponding value ranges. Furthermore, response surface analysis using the Box-Behnken (BB) test can further determine the optimal parameter combinations [13-15]. The results of these combinations can be utilized as input and training data in the process of solving the objective function.

For determining the objective function, the response surface methodology (RSM) [16-19] is commonly employed due to its ability to approximate complex functional relationships and reduce the likelihood of convergence to local optima. However, RSM often exhibits relatively poor robustness. In contrast, objective function based on the back propagation neural network algorithm (BPNN) [20-23] offers strong nonlinear mapping capability and reduced sensitivity to outliers compared with the RSM. Nevertheless, BPNN training is prone to premature convergence and entrapment in local optima. To compensate these deficiencies, the particle swarm optimization (PSO) algorithm can be utilized to enhance the training efficiency and prediction accuracy of the BPNN [24-26]. This hybrid PSO–BPNN approach enhances training efficiency and prediction accuracy, effectively avoids local optima, and improves overall model robustness, thereby enabling more accurate attainment of the requisite objective function.

After the determination of the objective function, evolutionary algorithms can be adopted to optimize its parameters. Commonly used

DOI: 10.5545/sv-jme.2025.1440

methods include PSO, ant colony algorithm, bee colony algorithm, differential evolution algorithm, and genetic algorithm (GA). Among them, PSO is characterized by simple parameter adjustments and fast convergence speed [27-29], yet its performance is highly sensitive to the initial parameter settings. In parameter optimization [30-32], the ant colony algorithm is particularly effective for combinatorial and dynamic optimization problems. The bee colony algorithm [33,34] exhibits strong robustness and global search capabilities, making it suitable for complex optimization environments. Differential evolution algorithm [35,36] demonstrates better performance in continuous parameter optimization. GA [37-40], with its mechanisms of population search, such as selection, crossover, and mutation, demonstrates outstanding global performance in avoiding local optima. Its global optimization capability has been validated in high-dimensional nonlinear parameter optimization [41]. For inverse problems characterized by multiple parameters and strong nonlinearity, such as the simulation of wet concrete particles, the global search capability and strong adaptability of GA are particularly suitable. Therefore, GA is ultimately selected in this study for global parameter optimization.

To address existing challenges in the calibration of discrete element method (DEM) parameters for wet particles, such as low efficiency in screening multi-dimensional parameters, limited capability of traditional fitting models, and the tendency of inverse solutions to converge to local optima, this paper integrates experimental design and intelligent algorithms to propose a systematic parameter calibration framework. The study focuses on wet concrete aggregates with a moisture content of 4 % to 6 %. Key influencing parameters are first identified through PB screening and steepest ascent experiments. Subsequently, representative sample data are obtained via BB test, and a PSO-BPNN combined with a GA is constructed to achieve global parameter optimization, enabling systematic calibration of critical parameters, such as particle shape, density, and surface energy. This research provides a high-precision, high-efficiency parameter calibration approach for DEM modeling of wet cohesive granular materials, holding positive significance for enhancing the simulation credibility of related equipment design and process optimization.

2 METHODS

To fulfill the objective of optimizing the simulation parameters of wet concrete particles, four parameters influencing the repose angle were initially selected, namely the coefficient of static friction (X_1), the coefficient of rolling friction (X_2), the surface energy (X_3), and the coefficient of restitution (X_4). Based on a review of relevant literature, the value ranges of the four parameters were preliminarily determined. Twelve sets of experiments were designed using the PB experiment to further screen out the most significant influences to the repose angle, namely X_1, X_2, and X_3. Subsequently, five sets of experiments were carried out using the steepest ascent experiment to determine the optimal value intervals of these three parameters. Finally, a total of 17 sets of experiments were conducted using the BB test for RSM analysis, obtaining a second-order regression model describing the relationship between the repose angle and selected parameters. The fitting status of the regression model was verified using the ANOVA method.

To determine the objective function, a PSO-BPNN model was constructed. From the initial 17 sets of experimental sample data, 80 % were randomly selected as training samples, while the remaining

Fig. 1. Flowchart of PSO-BP-GA optimization process

20 % were used as test samples. The training set was employed to train the NN model and optimize its parameters, whereas the test dataset was utilized to assess the generalization ability of the model.

In this paper, the extremum of an unknown nonlinear functions cannot be precisely identified solely from its input and output data. Hence, by integrating the nonlinear optimization capability of the GA, with the mean square error (MSE) of the PSO-BP model as the fitness function, and a packing angle of 32.07° as the target value, the coefficient of static friction (X_1), the coefficient of rolling friction (X_2), and the surface energy (X_3) were optimized. The overall optimization procedure is shown in Fig. 1. The number of iterations was set to 50, the population size to 10, and the crossover probability and the mutation probability to 0.4 and 0.2, respectively. The iteration number of 50 and population size of 10 were determined through sensitivity analysis to ensure sufficient convergence while maintaining reasonable computational efficiency. The crossover probability of 0.4 and mutation probability of 0.2 were selected based on commonly adopted GA parameter settings. These values, validated through preliminary experiments, effectively avoid local optima and promote population diversity.

2.1 Experimental Measurement of the Repose Angle

In this paper, the parameters between wet concrete particles were calibrated using a piling (angle of repose) test. The test device is shown in Fig. 2. The test apparatus consisted of a transparent cylindrical container made of organic glass, with diameter of 150 mm, and height of 300 mm. First, the cylinder was placed vertically on a horizontal plane and connected to a three-axis platform using a dedicated fixture to ensure alignment and stability. Then, a certain mass of wet concrete particles was filled into the cylinder. Finally, the *Z*-axis motor was activated to lift the cylinder at a constant speed of 300 mm/min. As the cylinder was raised, the wet concrete particles discharged freely from the bottom opening and formed a pile on the horizontal plane. When the particles stopped moving, photos of the formed particle pile were taken. The image acquisition system used an NPX-GS6500UM high-speed camera with a maximum resolution of 640×480.

MATLAB software was used to perform grayscale conversion and binarization of the particle pile images, extract the contour of the particle pile profile, and fit them to calculate the magnitude of the tangent value, thereby obtaining the contour inclination (repose) angle of the particle pile. Each group of experiments was repeated five times, obtaining a total of ten datasets. The measured repose angles and corresponding error analysis are summarized in Table 1. The coefficient of variation was calculated to be 3.23 %, which is less than 5 %, proving the measurement method as a reliable one. The final repose angle of the wet concrete particle pile was determined to be 32.07°. The contour extraction process is shown in Fig. 3.

Table 1. Repose angle measurement data and error analysis

No.	Repose angle [°]	Statistical measure	Value
1	30.61	Mean	32.07°
2	33.48	Median	32.00°
3	32.17	Sample standard deviation	1.0365°
4	31.83	Range	2.87°
5	33.29	Coefficient of variation	3.23 %
6	30.92	Standard error	0.3277°
7	33.04	95 % confident interval	(31.33°, 32.81°)
8	31.56		
9	32.74		
10	31.06		

2.2 Numerical Simulations of the Repose Angle

2.2.1 Contact Model Considering the Viscosity of Particles

This paper adopts the Hertz-Mindlin with JKR contact model implemented in the commercial software EDEM, also known as the JKR cohesion model, which is mainly applicable to powdery particles such as pharmaceutical powders, ores, soils and other wet materials [42]. This model effectively captures the adhesion and

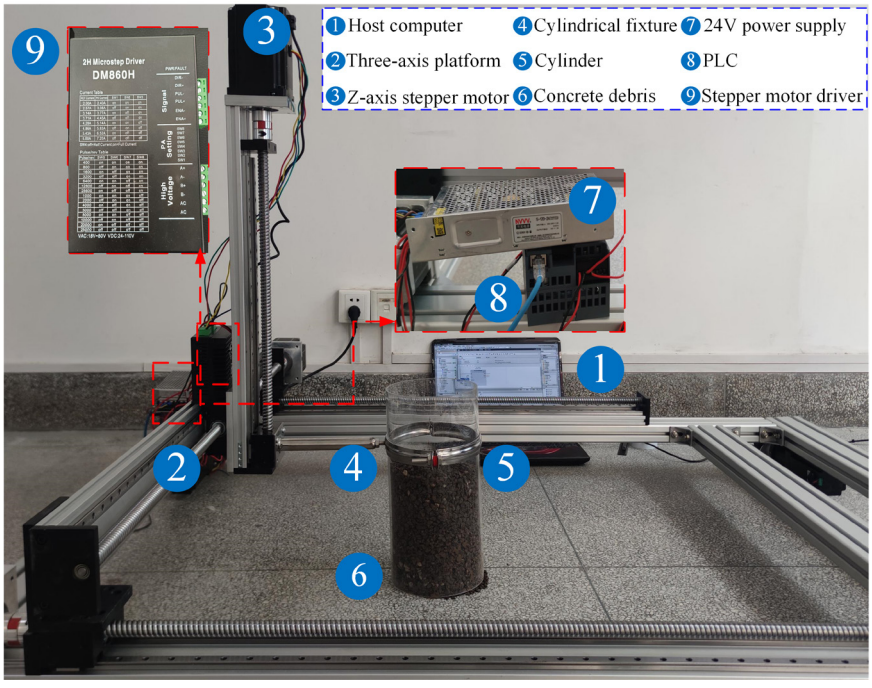

Fig. 2. Test device

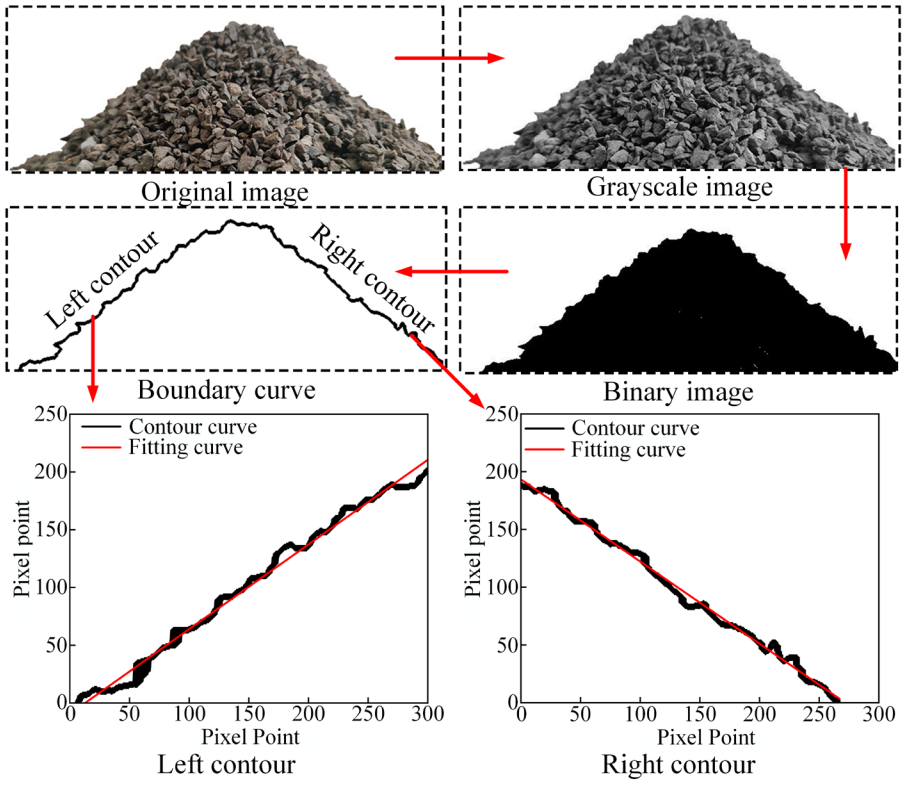

Fig. 3. Process of extracting the contour

agglomeration effects between particles due to electrostatic force and moisture content. The adhesion force between particles refers to the corresponding surface energy. The concrete particles are simplified and represented as spheres, as shown in Fig. 4.

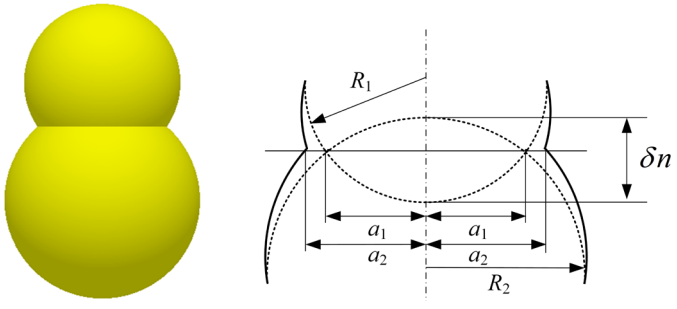

Fig. 4. JKR contact model

Due to the influence of surface energy, the contact radius between two particles expands from a_1 to a_2. The work of adhesion W, a key parameter, governing the adhesive force between different concrete particles, can be expressed as:

$$W = \gamma_1 + \gamma_2 - \gamma_{12}, \tag{1}$$

where, γ_1 represents the surface energy of particle 1; γ_2 the surface energy of particle 2; γ_{12} the interfacial surface energy between particle 1 and particle 2. When the particle materials are the same, the interfacial energy $\gamma_{12}=0$, that is, $\gamma_1=\gamma_2=\gamma$, thus the effect of adhesion between the same particles becomes $W = 2\gamma$.

The normal elastic contact force F_{JKR} of wet particles and the normal overlap are presented in Eqs. (2) and (3).

$$F_{JKR} = -4\sqrt{\pi\gamma E^* a_2^3} + \frac{4E^* a_2^3}{3R^*}, \tag{2}$$

$$\delta n = \frac{a_2^2}{R^*} - 2\sqrt{\frac{\pi\gamma a_2}{E^*}}, \tag{3}$$

where, γ represents the surface energy of the particles, E^* the equivalent elastic modulus, a_2 the radius of the contact surface after the collision of two particles, and R^* the equivalent contact radius. Among them:

$$\frac{1}{E^*} = \frac{1-v_1^2}{E_1} + \frac{1-v_2^2}{E_2}, \tag{4}$$

$$\frac{1}{R^*} = \frac{1}{R_1} + \frac{1}{R_2}, \tag{5}$$

where, E_1, v_1, and R_1 represent the elastic modulus, Poisson's ratio, and radius of particle 1, respectively; E_2, v_2, and R_2 represent the elastic modulus, Poisson's ratio, and radius of particle 2, respectively.

When the surface energy of the particles equals 0 J/m^2, the normal elastic contact force F_{JKR} of this model can be simplified to the contact force F_{Hertz} of the Hertz contact model, as expressed in Eq. (6):

$$F_{Hertz} = \frac{4}{3} E^* \sqrt{R^*} \delta^{\frac{3}{2}}. \tag{6}$$

2.2.2 Particle Packing Simulation Test

When conducting simulations in EDEM, it is essential to model particle behavior based on the actual morphology of concrete particles. However, the complex geometry of concrete fragments would significantly increase computational costs. Therefore, the particle shapes need to be appropriately simplified. Based on existing studies on particle shape characterization [43], this work focuses on four typical and geometrically representative shapes as research objects: flattened, conical, block-like and spherical. These shapes essentially capture the principal contours and contact characteristics

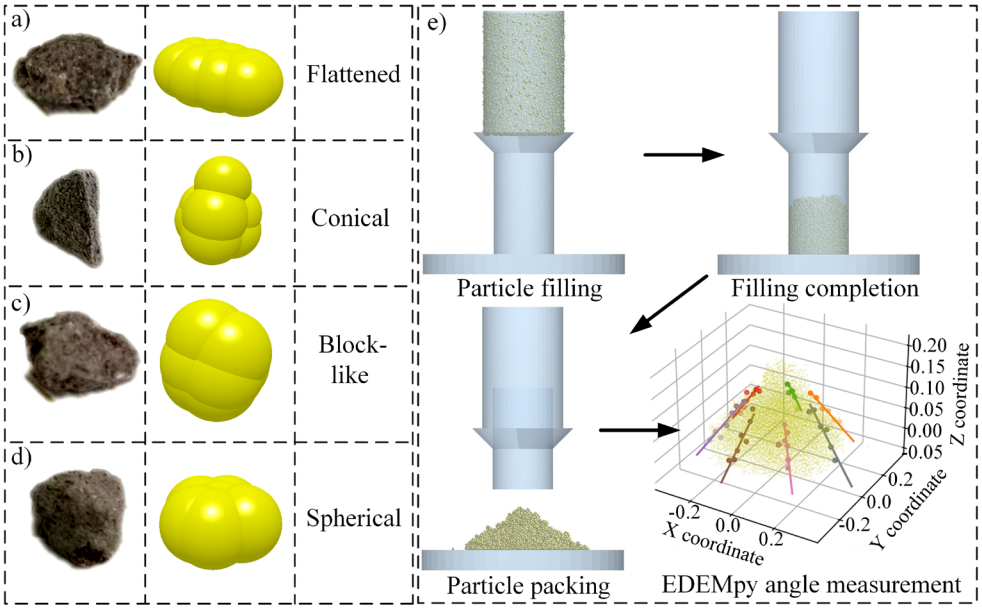

Fig. 5. Concrete particle shapes and the packing processes: a) flattened, b) conical, c) block-like, d) spherical, an e) packing process

of real fragments, thereby meeting the requirements for simulating accumulation behavior. Using the multi-sphere assembly approach based on spherical primitive elements, the non-spherical particles were constructed, as shown in Fig. 5. The particle diameters were maintained within the range of 3 mm to 5 mm.

The repose angle test was conducted in the numerical simulation using the established concrete fragment particle models . The cylinder sizes in the simulation test were consistent with those used in the physical experiments. The simulation procedure was as follows: First, a finite set of particles was defined, and a certain mass of concrete particles was generated in the container. After particle generation was completed and the particles reached a stable state, the cylinder was lifted upward at a constant speed of 300 mm/min. As the cylinder rose, the concrete particles began to fall and accumulate on the bottom plane, ultimately forming an approximately conical particle pile. Through EDEM post-processing, the simulation was terminated when the velocities of all particles were 0 m/s. The simulation time was set to 3 s, with a time step of 1×10^{-3} s. The simulation hardware included a central processing unit (CPU) model Intel(R) Xeon(R) W-2245 CPU @ 3.90 GHz, 3.91 GHz, and 32 GB of random-access memory (RAM).

After completing the accumulation simulation in EDEM, to repose angle was accurately determined using EDEMpy interface. The three-dimensional coordinates of all stationary particles were directly extracted, and the three-dimensional surface topography of the particle pile was reconstructed. Contour lines were then derived from the fitted surface, to calculate its inclination angle as the simulated repose angle. This method calculates the repose angle directly from the particle spatial data, thereby avoiding potential errors introduced by secondary image processing. Each group of simulation tests was repeated three times. The accumulation process obtained from the simulation is shown in Fig. 5e.

3 RESULTS AND DISCUSSION

3.1 Screening of Significant Parameters Through the PB experiment

In this study, based on existing literature [44-47] on similar materials, the value ranges for four key parameters, namely the coefficient of restitution, coefficient of static friction, coefficient of rolling friction, and surface energy, were preliminarily determined. The Design-Expert 13 software was used to design the PB experiment to evaluate the effects of these influencing factors and screen out the factors significantly affecting the repose angle. Each factor was set at two levels, high and low, resulting in a total of 12 experimental runs. The final ranges for the four parameters are shown in Table 2.

Table 2. Parameters of PB experiment

Symbol	Parameter	Low level (–1)	High level (+1)
X_1	Coefficient of static friction	0.05	0.5
X_2	Coefficient of rolling friction	0.03	0.4
X_3	Surface energy [J/m^2]	0.5	2
X_4	Coefficient of restitution	0.1	0.4

Table 3. PB experimental design and results

No.	X_1	X_2	X_3 [J/m^2]	X_4	Repose angle Y [°]
1	0.5	0.03	0.5	0.4	22.03
2	0.5	0.03	2	0.4	24.78
3	0.5	0.03	2	0.1	25.12
4	0.05	0.03	2	0.1	27.76
5	0.05	0.4	2	0.4	36.93
6	0.5	0.4	2	0.1	33.29
7	0.05	0.03	0.5	0.4	22.36
8	0.05	0.4	2	0.4	37.15
9	0.05	0.4	0.5	0.1	30.78
10	0.5	0.4	0.5	0.4	27.84
11	0.5	0.4	0.5	0.1	32.25
12	0.05	0.03	0.5	0.1	23.79

The PB experimental design and corresponding results are shown in Table 3, while ANOVA for the effect of the four parameters on the repose angle is shown in Table 4.

The results demonstrate that the P-values of the coefficient of static friction, the coefficient of rolling friction, and the surface energy between wet concrete particles are all less than 0.05 J/m^2, demonstrating that these parameters have a significant influence

Table 4. ANOVA of the PB experiment

Indicator	Source of variance	Sum of squares	Degrees of freedom	Mean square	F	P-value
Repose angle	Model	300.46	4	75.11	34.45	0.0001**
	Coefficient of static friction	15.10	1	15.10	6.92	0.0338*
	Coefficient of rolling friction	228.81	1	228.81	104.93	<0.0001**
	Surface energy [J/m^2]	56.25	1	56.25	25.79	0.0014**
	Coefficient of restitution	0.3008	1	0.3008	0.1380	0.7213
	Residual	15.26	7	2.18		
	Comprehensive	315.72	11			

Note: ** indicates extremely significant ($P < 0.01$), * indicates significant ($0.01 \leq P < 0.05$).

on the repose angle. In contrast, the P-value of the coefficient of restitution is 0.7213, which exceeds 0.05, indicating no significant effect. This behavior can be attributed to the dominance of adhesive forces in the wet concrete particle system. Under low-speed accumulation conditions, the slight rebound tendency following particle collisions is rapidly suppressed and dissipated by the strong surface energy in the JKR model. Consequently, its elastic recovery effect has a negligible impact on the final accumulation morphology. Furthermore, the coefficient of variation of the experimental data is 5.15 %, which is below 10 %, indicating good experimental stability. The adjusted coefficient of determination (R^2_{adj}) is 0.9240, signifying a high level of agreement between the regression model and the experimental data. In addition, the adequate precision value is 16.0584, which is significantly higher than the recommended minimum value of 4, further confirming the high reliability of the experiment.

3.2 Optimal Value Range of Significant Parameters Determined by Steepest Ascent Experiment

Based on the results of the PB experiment, the non-significant factor was set at its mid-level in subsequent experiments. Specifically, the coefficient of restitution was set to 0.2. For the three significant parameters identified through the PB experiment, appropriate gradient values were determined based on their relative influence strength. This allowed the experimental points to move along the steepest ascent direction on the predicted response surface, thereby efficiently approaching the optimal region. Accordingly, five groups of steepest ascent experiments were conducted. The corresponding experimental design and results are presented in Table 5.

Table 5. Design and results of the steepest ascent experiment

No.	X_1	X_2	X_3 [J/m^2]	Repose angle (Y) [°]	Relative error
1	0.05	0.03	0.5	18.08	44.95 %
2	0.112	0.122	0.875	23.67	27.92 %
3	0.275	0.215	1.25	34.24	4.26 %
4	0.438	0.308	1.625	42.51	29.45 %
5	0.5	0.4	2	46.85	42.66 %

The results show that the repose angle of the wet concrete particles increases with increasing values of X_1, X_2 and X_3. Meanwhile, the relative error between the simulated and experimentally measured angles of repose initially decreases and then increases. It can be obtained from Table 5, that Test 3 exhibits the minimum relative error of 4.26 %, indicating that the optimal response region is located near Level 3. Accordingly, the parameter ranges defined by the two adjacent experimental groups were taken as the value range for the BB test for conducting the RSM analysis test. Based on this, RSM regression model was established.

3.3 Response Surface Methodology (RSM)

Based on the results of the steepest ascent experiment, the BB test was employed for RSM to determine the optimal parameter combination. The parameter ranges of the steepest ascent experiment results were adopted as the upper and lower limits for the response surface analysis, while the non-significant parameters were fixed at the intermediate level. The coded factor levels used in the BB experimental design are shown in Table 6.

Table 6. Coded factor levels used in the BB experimental design

Level	X_1	X_2	X_3 [J/m^2]
Low level	0.112	0.122	0.875
Middle level	0.275	0.215	1.25
High level	0.438	0.308	1.625

According to Table 6, a BB response surface experiment with 17 runs was designed for three factors at three levels. This experimental design was employed to explore the influence of variables on the repose angle, and to calibrate and optimize the sensitive coefficients (coefficient of static friction, coefficient of rolling friction, and surface energy). The detailed BB experimental design and results are shown in Table 7.

The experimental results were analyzed using RSM. By taking the coefficient of static friction (X_1), the coefficient of rolling friction (X_2), and the surface energy (X_3) as independent variables, and the repose angle (Y) as the response value, the second-order multiple regression equation was obtained:

$$Y = 33.91 + 1.9X_1 + 5.99X_2 + 1.12X_3 - 1.37X_1X_2 + 0.105X_1X_3 - 1.52X_2X_3 + 1.54X_1^2 - 0.524X_2^2 - 0.584X_3^2. \quad (7)$$

The ANOVA was employed to validate the adequacy of the regression equation and to examine the statistical significance of the model, including the main effects and interaction effects of each factor. The results are presented in Table 8. The regression model exhibits $P < 0.0001$, indicating that the correlation between the independent variables and the response values of the model is highly significant. The P-value of the lack-of-fit term is 0.3225 ($P > 0.05$), suggesting the lack of fit is not significant relative to the pure error and that the regression model adequately represents the experimental data. The coefficient of determination (R^2 = 0.9783) and the adjusted R^2 (R^2_{adj} = 0.9503) are both close to 1, indicating excellent agreement between the computational model and experimental data. Furthermore, the difference between the R^2_{adj} and the predicted coefficient of determination (R^2_{pre}=0.7948) is less than 0.2, further supporting model reliability. Moreover, the adequate precision (21.2234>4) confirms the high dependability of the regression equation. Additionally, the effects of the coefficient of static friction and the coefficient of rolling friction between the wet

concrete particles exhibit extremely significant effects ($P<0.01$) on the repose angle.

Table 7. Design and results of BB test

No.	X_1	X_2	X_3 [J/m^2]	Repose angle Y [°]
1	0.438	0.215	1.625	37.85
2	0.112	0.122	1.25	25.59
3	0.275	0.122	1.625	30.36
4	0.275	0.215	1.25	34.93
5	0.275	0.122	0.875	24.13
6	0.112	0.215	1.625	33.15
7	0.112	0.215	0.875	32.09
8	0.275	0.308	0.875	38.27
9	0.438	0.308	1.25	41.53
10	0.438	0.122	1.25	31.43
11	0.112	0.308	1.25	41.15
12	0.275	0.215	1.25	34.24
13	0.275	0.215	1.25	34.37
14	0.275	0.215	1.25	33.53
15	0.438	0.215	0.875	36.37
16	0.275	0.308	1.625	38.44
17	0.275	0.215	1.25	32.47

3.4 Influence of Interaction Factors on the Repose Angle

When the remaining factors were fixed at their median values, contour plots of each interaction term and the response surface of the interaction relative to the repose angle were depicted using Design-Expert 13. These plots enable a visual assessment of the interaction effects between pairs of factors. As shown in Fig. 6, the curve graphs indicate the existence of a nonlinear relationship between influencing factors and the repose angle. Fig. 6a presents the response surface describing the interaction between the coefficient of static friction (X_1) and the coefficient of rolling friction (X_2) . Compared with X_1 direction, the response surface exhibits a steeper gradient along the X_2 direction, suggesting that the influence of X_1 on the repose angle is relatively smaller than that of X_2. Fig. 6b is the response graph of the interaction between the coefficient of static friction (X_1) and the surface energy (X_3). Through the contour plot, it can be observed that there is no significant interaction between X_1 and X_3. In this case X_1 has a greater influence on the repose angle than X_3. Fig. 6c shows the interaction between the coefficient of rolling friction (X_2) and the surface energy (X_3) . The response surface curve reveals a steeper slope along X_2 axis than along X_3 axis, indicating that the contribution of X_2 to the repose angle is more significant than that of X_3. By comparing Figs. 6a and c, it can be stated that the relative influence of the three factors on the repose angle follows the order: $X_2>X_1> X_3$, which is consistent with the result of the ANOVA.

3.5 Optimal Model

3.5.1 Establishment of the PSO-BP Model

To improve the prediction performance of the BPNN and avoid its tendency to fall into local optima, we used the PSO algorithm to globally optimize its initial weights and thresholds [48]. This optimization process maps the parameters to be optimized in the BP network to the position of each particle within the swarm. By iteratively evaluating the network prediction error corresponding to parameter combinations and tracking both individual and group historical optimal solutions, the qwarm search is dynamically guided toward optimal regions of the solution space.

To construct the PSO-BPNN model, 80 % of the sample data was used as the training, and the remaining 20 % was reserved for testing. The parameters for the PSO algorithm were set as follows: the population size was set to 10 to balance computational efficiency and global search capability; the maximum number of iterations was set to 30, determined through convergence testing to ensure algorithm stability within a reasonable timeframe; the particle position range was set between [–2, 2], and the particle velocity range was set to [-0.5, 0.5] to avoid premature convergence; the inertia weight was set to 0.6, and the acceleration constants c_1 and c_2 were both set to 2 to promote a balance between exploration and exploitation; the maximum number of training epochs was set to 100, the learning

Table 8. The ANOVA results of the BB test

Source	Sum of squares	Degree of freedom	Mean square	F	P-value	Significance
Model	354.12	9	39.35	34.98	<0.0001	Significant
X_1 Coefficient of static friction	28.88	1	28.88	25.68	0.0015**	
X_2 Coefficient of rolling friction	286.56	1	286.56	254.80	<0.0001**	
X_3 Surface energy [J/m^2]	9.99	1	9.99	8.88	0.0205*	
X_1X_2	7.45	1	7.45	6.63	0.0368*	
X_1X_3	0.0441	1	0.0441	0.0392	0.8487	
X_2X_3	9.18	1	9.18	8.16	0.0244*	
X_1^2	10.00	1	10.00	8.89	0.0205*	
X_2^2	1.16	1	1.16	1.03	0.3444	
X_3^2	1.44	1	1.44	1.28	0.2957	
Residual	7.87	7	1.12			
Lack of fit	4.29	3	1.43	1.60	0.3225	Insignificant
Pure error	3.58	4	0.8947			
Cor total	361.99	16				
R^2	0.9783					
R^2_{adj}	0.9503					
R^2_{pre}	0.7948					
Adequate precision	21.2234					

Note: ** indicates extremely significant ($P < 0.01$), and * indicates significant ($0.01 \leq P < 0.05$)

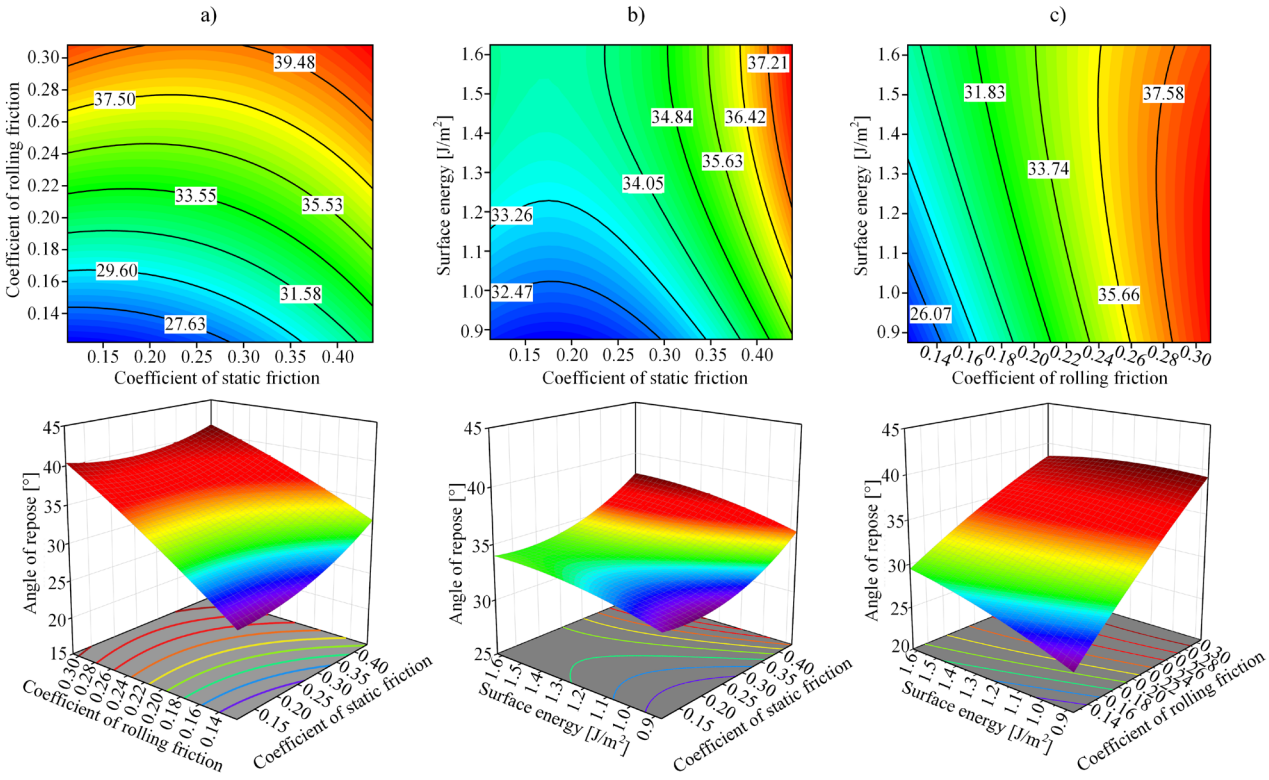

Fig 6 . Influence of interaction factors on repose angle; a) contour plot and response surface of X_1 and X_2, b) contour plot and response surface of X_1 and X_3, and c) contour plot and response surface of X_2 and X_3

rate was set to 0.01, and the minimum training error target was set to 10^{-5}. These parameters were selected according to the training requirements of the BPNN and further optimized through trial and error to minimize prediction error.

Figure 7 presents the relationship between the network output values and the objective functions of the training, test, and complete sets. The results indicate that the correlation coefficients R of all datasets exceed 0.95, with no overfitting phenomenon occurring, suggesting that the model's good generalization performance.

3.5.2 Comparison of Models

This study compares the prediction performance of RSM, BP and PSO-BP. The comparison graph between the predicted and actual values for each model is shown in Fig. 8a. The correlation coefficient R was calculated to evaluate the predictive accuracy of each model. The results show that the PSO-BP achieves the highest correlation cofficient, which is 0.9921, suggesting that the PSO-BPNN model outperforms the RSM and BPNN models in terms of prediction accuracy, stability and generalization capability. Fig. 8b represents the comparison curves of the fitting results obtained from the three models.

To assess the predictive performance of the different models, the coefficient of determination (R^2), mean square error (*MSE*), and average absolute deviation (*AAD*) were adopted as evaluation metrics. A higher R^2 value closer to 1, together with the lower the *MSE* and *AAD* values, indicates better predictive accuracy of the model. The calculations of each evaluation index are provided in Eqs. (8) to (10).

$$R^2 = 1 - \frac{\sum_{i=1}^{n}(Y_i - \hat{Y}_i)^2}{\sum_{i=1}^{n}(Y_i - \bar{Y})^2}, \tag{8}$$

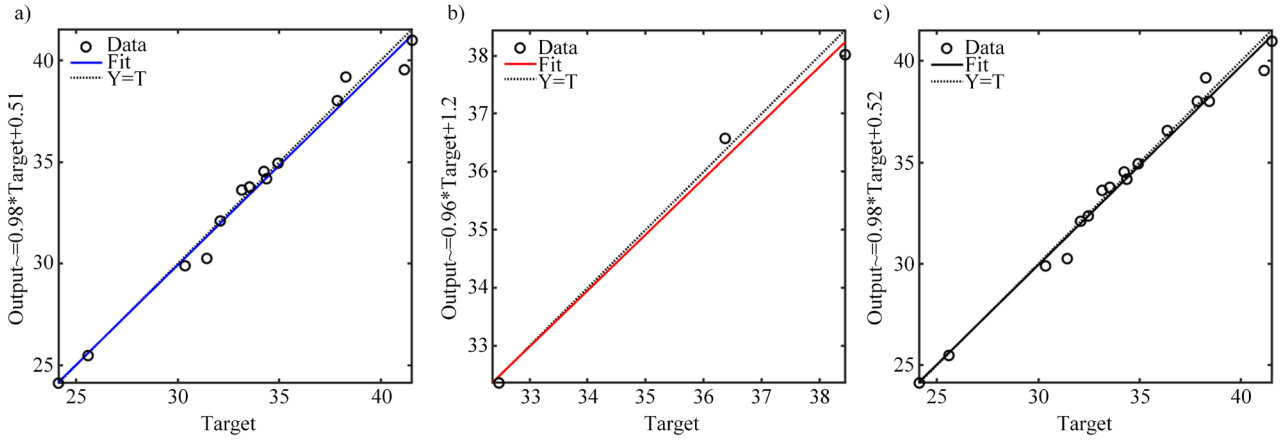

Fig. 7. Fitting plot of predicted values and expected output values; a) training at R = 0.99176, b) test at R = 0.99495, and c) all at R = 0.99213

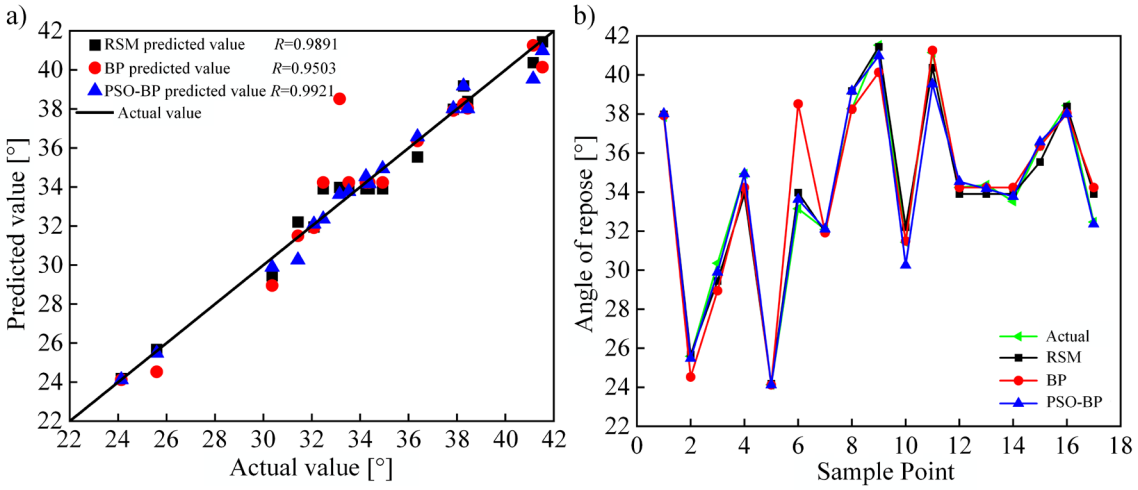

Fig. 8. Comparison of predicted values and fitting results of different models; a) predicted values, b)fitting results

$$MSE = \frac{1}{n}\sum_{i=1}^{n}(Y_i - \hat{Y}_i)^2, \tag{9}$$

$$AAD = \frac{1}{n}\sum_{i=1}^{n}\left|Y_i - \hat{Y}_i\right|, \tag{10}$$

where n is the number of samples, $\hat{Y}_i$ and Y_i are predicted and actual value of i^{th} sample, respectively; and $\overline{Y}$ is the mean of the actual values. The comparative results of prediction accuracy among different models are presented in Table 9.

Table 9. Comparison of prediction accuracy among different models

Prediction model	R^2	*MSE*	*AAD*
RSM	0.9503	0.4631	0.5419
BP	0.9031	2.2467	0.7886
PSO-BP	0.9830	0.3530	0.4087

As indicated in Table 9, the R^2 value of the PSO-BP model is closer to 1 compared to the other two models, while its *MSE* and *AAD* values are significantly lower. This demonstrates that PSO-BP effectively decreases prediction error and achieves a better fit between the predicted and actual values. This advantage stems from the global search capability of PSO algorithm. The algorithm uses prediction error as the fitness function, performs parallel optimization in the solution space, and provides the BP network with a set of initial weights and thresholds that are close to the global optimum. This effectively overcomes the inherent limitation of standard BP, where gradient descent is prone to falling into local optima, enabling more stable and accurate convergence performance in strongly nonlinear parameter inversion for wet concrete.

3.5.3 Parameter Optimization Using PSO-BP-GA

Based on the established PSO-BPNN prediction model, the ranges of each input parameter and the optimization target were determined. GA was then employed to optimize the model parameters. To obtain the optimal combination of parameters, with 32.07° as the optimization objective, the objective function and constraint function of the established optimization problem are defined as follows:

$$\begin{cases} Y = (X_1, X_2, X_3) = 32.07 \\ s.t. \begin{cases} 0.112 \le X_1 \le 0.438 \\ 0.122 \le X_2 \le 0.308 \\ 0.875 \le X_3 \le 1.625 \end{cases} \end{cases}. \tag{11}$$

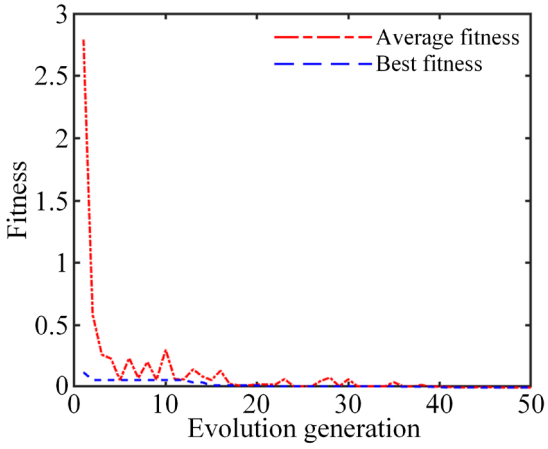

Fig. 9. Fitness evolution curve with termination generation at 50

Fig. 9 illustrates the evolution of fitness value with respect to the evolutionary generations. The fitness is defined as the root mean square error (*RMSE*) between the predicted value and the target value. In the initial stage, the GA rapidly reduces the fitness via population-based search. Subsequently, as crossover and selection operations are performed, the fitness fluctuates within a narrow range and gradually approaches the target value. By the 17th generation, the fitness curve tends to converge, suggesting a substantial reduction in the disparity between the predicted and target values. When the number of iterations reaches 50, the GA terminates and outputs the optimal individual, obtaining the optimal parameters: the coefficient of static friction of 0.158, the coefficient of rolling friction of 0.187, and the surface energy of 1.580 J/m^2.

3.6 Validations

The optimized parameter values obtained were imported into EDEM to conduct the simulation test of the repose angle. Five independent simulations were carried out to simulate the accumulation behavior of concrete particles. The repose angles obtained by EDEMpy were 31.73°, 32.64°, 32.96°, 32.17°, and 32.05° respectively. The average repose angle was 32.31°, showing a relative error of only 0.748 % compared with the experimental mean value. As shown in Fig. 10, a comparison between the simulation results and the exparimetal

observations show no significant discrepancy between the repose angle or the particle accumulation morphology. These results verify the accuracy of the optimized parameters.

Fig. 10. Comparison of a) actual repose angle, and b) simulated repose angle

4 CONCLUSIONS

1. The PB experiment and steepest ascent experiment were employed to screen out the significant factors (coefficient of static friction, coefficient of rolling friction and surface energy among wet concrete particles) that affect repose angle, and to further narrow the range of significant parameter values.
2. By comparing the performance metrics (R^2, *MSE*, and *AAD*) of the RSM, BP, and PSO-BP models, the PSO-BP model was found to exhibit superior predictive performance, achieving the highest R^2 value (0.9830) , and the lowest *MSE* (0.3530) and *AAD* (0.4087). This indicates that BP optimized by PSO can effectively reduce the prediction error and demonstetes higher predictive ability and fitting stability.
3. The GA was employed to conduct the inverse function optimization based on the established PSO-BP model, resulting optimal contact parameters for wet concrete particles: a static friction coefficient of 0.158, a rolling friction coefficient of 0.187, and a surface energy of 1.580 J/m^2. The average repose angle value of the five measured simulation was 32.31°, with a relative error of only 0.748 %. Therefore, the PSO-BP-GA method is effective for high-precision calibration of wet concrete contact parameters.

In summary, this study proposes a hybrid calibration framework that integrates experimental design, response surface analysis, and intelligent algorithm optimization. This method efficiently identifies key parameters through experimental design, utilizes the PSO-BP model to establish a complex nonlinear mapping relationship between contact parameters and the repose angle, and employs GA to achieve global inversion optimization. Validation results indicate that this method can efficiently and accurately determine discrete element contact parameters for wet concrete, providing a reliable solution for calibrating discrete element parameters of wet cohesive particle systems and significantly enhancing the accuracy and reliability of DEM parameter calibration.

References

[1] Yan, D.X., Yu, J.Q., Liang, L.S., Wang, Y., Yu, Y.J., Zhou, L., et al. A comparative study on the modelling of soybean particles based on the discrete element method. *Processes* 9 286 (2021) **DOI:10.3390/pr9020286**.

[2] Yan, D.X., Yu, J.Q., Wang, Y., Sun, K., Zhou, L., Tian, Y., et al. Measurement and calibration of DEM parameters of soybean seed particles. *Agric (Basel)* 12 1825 (2022) **DOI:10.3390/agriculture12111825**.

[3] Xu, T.Y., Fu, H., Liu, M., Feng, W.Z., Zhang, R.X., Wang, Y., Ellipsoidal seed modeling and simulation parameter selection based on the discrete element method. *Mater Today Commun* 37 106923 (2023) **DOI:10.1016/j.mtcomm.2023.106923**.

[4] Ajmal, M., Roessler, T., Richter, C., Katterfeld, A. Calibration of cohesive DEM parameters under rapid flow conditions and low consolidation stresses. *Powder Technol* 374 22-32 (2020) **DOI:10.1016/j.powtec.2020.07.017**.

[5] Washino, K., Chan, E.L., Faroux, D., Tsuji, T., Takahashi, T., Sasabe, S. On DEM simulation of loose packing behaviour of fine and cohesive particles. *Adv Powder Technol* 36 104809 (2025) **DOI:10.1016/j.apt.2025.104809**.

[6] Coetzee, C.J., Scheffler, O.C. Review: The calibration of dem parameters for the bulk modelling of cohesive materials. *Processes* 11 5 (2023) **DOI:10.3390/pr11010005**.

[7] Choi, Y., Park, S., Park, C., Kim, D., Kim, Y. Meta-anova: Screening interactions for interpretable machine learning. *J Korean Stat Soc* 54 478-495 (2025) **DOI:10.1007/s42952-024-00302-2**.

[8] Mohsenijam, A., Siu, M.F.F., Lu, M. Modified stepwise regression approach to streamlining predictive analytics for construction engineering applications. *J Comput Civ Eng* 31 (2017) **DOI:10.1061/(asce)cp.1943-5487.0000636**.

[9] Yu, Z.Y., Xiong, W., Zhu, D.Q., Xue, K., Zhang, S., Kuang, F.M., et al. Analysis and calibration of parameters of wet-viscous paddy mud particles based on the slump experiment. *Inmateh-Agric Eng* 68 177-190 (2022) **DOI:10.35633/inmateh-68-18**.

[10] Zhang, J.X., Wang, Q.Y., Niu, F.S., Yu, X.D., Chang, Z.J., Wu, F., et al. Simulation and verification of discrete element parameter calibration of pulverized coal particles. *Int J Coal Prep Util* 45 1244-1263 (2025) **DOI:10.1080/19392699.2024.2379405**.

[11] Fang, W.Q., Wang, X.Z., Han, D.L., Chen, X.G. Review of material parameter calibration method. *Agric (Basel)* 12 706 (2022) **DOI:10.3390/agriculture12050706**.

[12] Shi, Z.L., Wang, M.J., Zhang, X.J., Cheng, J.P., Lu, D.M. Calibration and optimization of discrete element parameters for coated cotton seeds. *Eng Agric* 44 (2024) **DOI:10.1590/1809-4430-Eng.Agric.v44e20230085/2024**.

[13] Yang, L.Y., Chen, W.H., Kan, Z., Meng, H.W., Qi, J.T. Parameter calibration for discrete element simulation of leymus chinensis seeds based on RSM optimization. *Sci Rep* 15 7947 (2025) **DOI:10.1038/s41598-025-89181-z**.

[14] Yang, L., Li, J.W., Lai, Q.H., Zhao, L.L., Li, J.J., Zeng, R.H., Discrete element contact model and parameter calibration for clayey soil particles in the southwest hill and mountain region. *J Terramech* 111 73-87 (2024) **DOI:10.1016/j.jterra.2023.10.002**.

[15] Athijayamani, A., Ganesamoorthy, R., Loganathan, K.T., Sidhardhan, S. Modelling and analysis of the mechanical properties of agave sisalana variegata fibre/vinyl ester composites using Box-Behnken design of response surface methodology. *Stroj Vestn-J Mech E* 62 273-280 (2016) **DOI:10.5545/sv-jme.2015.2641**.

[16] Ren, J.Q., Xiao, M., Liu, G.Q. Rock macro-meso parameter calibration and optimization based on improved BP algorithm and response surface method in PFC 3D. *Energies* 15 6290 (2022) **DOI:10.3390/en15176290**.

[17] Tang, X.X., Yue, Y.H., Shen, Y.S. Prediction of separation efficiency in gas cyclones based on RSM and GA-BP: Effect of geometry designs. *Powder Technol* 416 118185 (2023) **DOI:10.1016/j.powtec.2022.118185**.

[18] Wang, C.Y., Wang, G.C., Shen, C.E. Analysis and prediction of grind-hardening surface roughness based on response surface methodology-BP neural network. *Appl Sci (Basel)* 12 12680 (2022) **DOI:10.3390/app122412680**.

[19] Chehreghani, S., Noaparast, M., Rezai, B., Shafaei, S.Z. Bonded-particle model calibration using response surface methodology. *Particuology* 32 141-152 (2017) **DOI:10.1016/j.partic.2016.07.012**.

[20] Li, X.Y. Application of particle swarm optimization algorithm in computer neural network. *Int Conf Comp Syst Electr Contr* 446-449 (2017).

[21] Cao, G.D., Su, H.W., Xie, S., Li, Z.G., Deng, D.Q., Jiang, S.Q., et al. Numerical investigation on pumping behavior of fresh concrete by CFD-DEM, considering uneven distribution of aggregate. *Constr Build Mater* 465 140130 (2025) **DOI:10.1016/j.conbuildmat.2025.140130**.

[22] Qi, J.T., Zhao, W.W., Kan, Z., Meng, H.W., Li, Y.P. Parameter optimization of double-blade normal milk processing and mixing performance based on RSM and BP-GA. *Food Sci Nutr* 7 3501-3512 (2019) **DOI:10.1002/fsn3.1198**.

[23] Jin, Z.J., Cheng, G., Xu, S.C., Yuan, D.P. Error prediction for a large optical mirror processing robot based on deep learning. *Stroj Vestn-J Mech E* 68 175-184 (2022) **DOI:10.5545/sv-jme.2021.7455**.

[24] Li, H.X., Li, G., Huang, Z.Y., Chen, M., Application of BP neural network based on genetic algorithm optimization. *Int Conf Intell Info Process* (2019) 160-165.

[25] Xia, Q.J., Ji, Y.C. Study on frost resistance of recycled rubber straw concrete using particle swarm optimization enhanced artificial neural networks. *Polymers* 16 3191 (2024) **DOI:10.3390/polym16223191**.

[26] Pan, X.P., Niu, Y.W., Zhao, Y., Huang, P.M., Wu, Y.Z. Parameter calibration method of clustered-particle logic concrete dem model using BP neural network-particle swarm optimisation algorithm (BP-PSO) inversion method. *Eng Fract Mech* 292 (2023) **DOI:10.1016/j.engfracmech.2023.109659**.

[27] Zhang, X.Y., Li, Y., Chu, G.S. Comparison of parallel genetic algorithm and particle swarm optimization for parameter calibration in hydrological simulation. *Data Intell* 904-922 (2023) **DOI:10.1162/dint_a_00221**.

[28] Rojas-Delgado, J., Núñez, V.M., Trujillo-Rasúa, R., Bello, R. Continuous hyper-parameter configuration for particle swarm optimization via auto-tuning. *Iberoam Congr Pattern Recognit* 458-468 (2019).

[29] Isiet, M., Gadala, M. Self-adapting control parameters in particle swarm optimization. *Appl Soft Comput* 83 105653 (2019) **DOI:10.1016/j.asoc.2019.105653**.

[30] Chen, Y.B., Guo, Z., Liu, J.G. An improved ant colony algorithm for PID parameters optimization. *Int Conf Intell Comput Technol Autom* 157-160 (2009) **DOI:10.1007/978-3-030-33904-3_43**.

[31] Fidanova, S., Roeva, O. Influence of ant colony optimization parameters on the algorithm performance. *Int Conf Large-Scale Sci Comput* 358-365 (2017).

[32] Abdelbar, A.M., Salama, K.M. Parameter self-adaptation in an ant colony algorithm for continuous optimization. *IEEE Access* 7 18464-18479 (2019) **DOI:10.1109/access.2019.2896104**.

[33] Zhi, D. Optimization of PID controller for single phase inverter based on ABC. *Int Conf Control Autom Robot* 501-504 (2019) **DOI:10.1007/978-3-319-73441-5_38**.

[34] Abhijith, Srinivasa, P., Grynal, D., Gautama, H. Surface roughness optimization in machining of az31 magnesium alloy using ABC algorithm. *Int Conf Res Mech Eng Sci* 144 03306 (2017) **DOI:10.1051/matecconf/201814403006**.

[35] Bäck, T.H.W., Kononova, A.V., van Stein, B., Wang, H., Antonov, K.A., Kalkreuth, R.T. et al. Evolutionary algorithms for parameter optimization-thirty years later. *Evol Comput* 31 81-122 (2023) **DOI:10.1162/evco_a_00325**.

[36] Pan, J.S., Yang, C., Meng, F.J., Chen, Y.X., Meng, Z.Y. A parameter adaptive DE algorithm on real-parameter optimization. *J Intell Fuzzy Syst* 38 5775-5786 (2020) **DOI:10.3233/jifs-179665**.

[37] Liu, Z.M., Li, C.Q., Feng, K., Application research of bp neural network optimized by genetic algorithm and particle swarm optimization algorithm in mbr simulation. *Int Conf Artif Intell Big Data* 119-123 (2019) **DOI:10.1109/ICAIBD.2019.8837011**.

[38] Li, G.H., Ma, J., Tian, X., Zhao, C., An, S.G., Guo, R. et al. Discrete meta-simulation of silage based on RSM and GA-BP-GA optimization parameter calibration. *Processes* 11 2784 (2023) **DOI:10.3390/pr11092784**.

[39] Chen, Y.P., Wu, H.X. Fuzzy neural network controller based on hybrid ga-bp algorithm. *Int Conf Comput Control Ind Eng* 335-339 (2013) **DOI:10.4028/www.scientific.net/AMR.823.335**.

[40] Zhao, M.J., Fang, J.J., Zhang, L., Dai, Z., Yao, Z.W. Improving the estimation accuracy of copper oxide leaching in an ammonia-ammonium system using RSM and GA-BPNN. *Russ J Non-Ferrous Metals* 58 591-599 (2017) **DOI:10.3103/s1067821217060177**.

[41] Liu, J., Liu, J., Gao, K., Mohagheghian, I., Fan, W., Yang, J., et al. A bioinspired gradient curved auxetic honeycombs with enhanced energy absorption. *Int J Mech Sci* 291-292 110189 (2025) **DOI:10.1016/j.ijmecsci.2025.110189**.

[42] Ma, G.G., Sun, Z.J., Ma, H., Li, P.C. Calibration of contact parameters for moist bulk of shotcrete based on EDEM. *Adv Mater Sci Eng* 2022 6072303 (2022) **DOI:10.1155/2022/6072303**.

[43] E, D., Wen, Y., Wu, Y., Li, J., Sun, W., Liu, Y., et al. Hydrodynamics of heterogeneous particle swarms in gas-liquid-solid stirred tanks with free surface studied by DEM-VOF. *Powder Technol* 462 121103 (2025) **DOI:10.1016/j.powtec.2025.121103**.

[44] Ma, H., Zhou, L., Liu, Z., Chen, M., Xia, X., Zhao, Y. A review of recent development for the CFD-DEM investigations of non-spherical particles. *Powder Technol* 412 117972 (2022) **DOI:10.1016/j.powtec.2022.117972**.

[45] Ma, H., Ma, G., Sun, Z., Gao, K., Chen, L. Study on flow characteristics of pneumatic conveying of stiff shotcrete materials by CFD-DEM. *Results Eng* 26 105129 (2025) **DOI:10.1016/j.rineng.2025.105129**.

[46] Li, Z.Q., Chen, H.M., Wu, Y.K., Xu, Z.H., Shi, H.Y., Zhang, P. CFD-DEM analysis of hydraulic conveying of non-spherical particles through a vertical-bend-horizontal pipeline. *Powder Technol* 434 119361 (2024) **DOI:10.1016/j.powtec.2024.119361**.

[47] Qi, L., Liu, C., Cui, W., Li, Y. Calibration of contact parameters of dem for fresh self-compacting concrete. *J Funct Mater* 49 7050-7056 (2018) **DOI:10.3969/j.issn.1001-9731.2018.07.008**.

[48] Zhang, Y., Wang, Z., Xi, M., Zhao, Y., Liu, J. Data-driven prediction of residual flexural capacity in corroded RC beams using PSO and GA-optimized CatBoost ensemble models. *Eng Res Express* 7 035129 (2025) **DOI:10.1088/2631-8695/adfcb3**.

Acknowledgment *This research is supported by the National Natural Science Foundation of China (52375080) and Key Research and Development Project in Shaanxi Province(2024GX-YBXM-247).*

Received: 2025-06-20, **revised:** 2025-12-17, **accepted:** 2025-12-22 *as Original Scientific Paper.*

Declaration of interests *The authors declare that they have no known competing financial interests or personal relationships that could have appeared to influence the work reported in this paper.*

Data availability *The data that support the findings of this study are available from the corresponding author upon reasonable request,*

Authors contribution *Xiaohui Liu: Conceptualization, Formal analysis, Methodology, Funding acquisition, Project administration, Writing–review & editing; Siyu Dong: Data curation, Investigation, Software, Validation, Writing-original draft; Kaidong Xue: Investigation, Methodology, Software, Validation, Writing-original draft; Penghui Wang: Software, Writing–review & editing; Yongyi Ren: Writing–review & editing.*

Optimizacija simulacijskih parametrov mokrih betonskih delcev na osnovi metode odzivne površine in metode PSO-BP-GA

Povzetek *Za reševanje izzivov nizke učinkovitosti umerjanja in omejene natančnosti pri diskretnem večparametričnem modeliranju posedanja mokrega betona, je bila v tej študiji razvita shema umerjanja parametrov, ki združuje načrtovanje eksperimentov in inteligentne algoritme. S tem je bila dosežena učinkovita in visoko natančna optimizacija inverzne funkcije za določitev kontaktnih parametrov, kar predstavlja zanesljivo osnovo za sorodne inženirske simulacije. Najprej je bil z eksperimentom poseda določen kot naravnega poseda mokrega betona, ki znaša 32,07 °. Z uporabo Plackett–Burmanovega (PB) eksperimenta in eksperimenta najstrmejšega vzpona so bili identificirani trije parametri z največjim vplivom na kot naravnega poseda mokrega betona ter njihova optimalna območja vrednosti: statični koeficient trenja (X_1), koeficient kotalnega trenja (X_2) in površinska energija (X_3). Nato je bilo z Box–Behnkenovim (BB) eksperimentalnim načrtom določenih 17 optimalnih kombinacij podatkov za te tri ključne parametre. Za vzpostavitev ciljne funkcije med kotom naravnega poseda mokrega betona in vplivnimi parametri ter za pridobitev optimalnih vrednosti parametrov je bila uporabljena metoda roja delcev, povratnega širjenja in genetskega algoritma (PSO-BP-GA). Najprej je bilo 80 % izmed 17 nizov podatkov, pridobljenih z BB-testom, uporabljenih kot učni vzorci za nevronsko mrežo s povratnim širjenjem (BPNN), preostalih 20 % pa kot testni vzorci. Nato je bil algoritem PSO uporabljen za optimizacijo uteži in pragov znotraj BPNN. Po določitvi ciljne funkcije je bil genetski algoritem (GA) uporabljen za inverzno optimizacijo, pri čemer je bil ciljni kot naravnega nasipa 32,07 °. Končno so bile določene optimalne vrednosti parametrov: statični koeficient trenja med delci mokrega betona (X_1) 0,158, koeficient kotalnega trenja (X_2) 0,187 in površinska energija (X_3) 1,580 J/m^2. Na podlagi teh parametrov je bilo izvedenih pet simulacij, pri čemer je bil povprečni izračunani kot naravnega poseda 32,31 °. V primerjavi z dejansko vrednostjo je relativna napaka znašala 0,748 %.*

Ključne besede *mokri betonski delci, optimizacija parametrov simulacije delcev, analiza odzivne površine, PSO-BP-GA*